J Solid State Electrochem (2005) 9: 267–276
DOI 10.1007/s10008-004-0596-8

ORIGINAL ARTICLE

D. Malevich · J. Li · M. K. Chung · C. McLaughlin
M. Schlaf · J. Lipkowski

In situ IR reflectance absorption spectroscopy studies of the effect of Nafion on CO adsorption and electrooxidation at Pt nanoparticles

Received: 18 August 2004 / Revised: 26 September 2004 / Accepted: 4 October 2004 / Published online: 10 December 2004

Abstract We have synthesized colloidal Pt nanoparticles with a mean particle size of 2.6 ± 0.4 nm by reducing $PtCl_2$ dissolved in *N*,*N*-dimethylacetamide with *t*-$BuMe_2SiH$. The latter compound acted both as a reducing agent and a stabilizer of the Pt nanoparticles. Pt nanoparticles were deposited onto the Au substrate and IR reflectance absorption spectroscopy (IRRAS) was applied to investigate CO adsorption and oxidation at the surface of the catalyst. The reactivity of the catalyst covered with Nafion was compared with the reactivity of the catalyst without Nafion. In addition, the reactivity of the colloidal Pt was compared with the reactivity of bulk polycrystalline Pt. We found that CO oxidation proceeds at lower over-potentials at nanoparticles than at polycrystalline Pt. The IRRAS data indicate that the difference in the reactivity may be explained by a different mechanism of the oxidation reaction; Langmuir–Hinshelwood at Pt nanoparticles and island formation and growth at polycrystalline Pt. We have also observed that a film of Nafion slows down the CO oxidation reaction. The IRRAS spectra for CO adsorbed at Pt nanoparticles covered by Nafion were significantly different from the spectra recorded for the nanoparticles in the absence of Nafion. The spectroscopic features suggest that in the presence of Nafion the nanoparticles experience regions of lower and higher proton concentration.

This paper is dedicated to Prof. G. Horanyi on the occasion of his 70th birthday and in recognition of his contribution to electrochemistry.

D. Malevich (✉) · J. Li · M. K. Chung · C. McLaughlin
M. Schlaf · J. Lipkowski (✉)
Department of Chemistry, University of Guelph, Guelph, ON, N1G 2W1, Canada
E-mail: dmalevic@uoguelph.ca
E-mail: jlipkows@uoguelph.ca

Introduction

Electrocatalytic properties of nanoparticles of platinum and platinum group metals have been investigated for several decades. Owing to their application as catalysts in low-temperature fuel cells, they continue to be a focus of a significant scientific interest. Poor CO tolerance is one of the major problems impeding the performance of low-temperature fuel cells [1]. CO is a well-known catalyst poison, irreversibly adsorbing on the Pt surface and dramatically slowing down surface reactions. The CO–Pt surface complex is an intermediate product of methanol electrooxidation in the direct methanol fuel cell [2]. Moreover, as a result of hydrocarbon reformation, CO is the major impurity present in the hydrogen fuel fed into the polymer electrolyte membrane fuel cell [3]. A number of approaches have been used to improve CO tolerance of the Pt catalyst, such as alloying Pt with one [4–12] or several [13, 14] elements, optimizing the nanoparticle size [15–22] or surface modification by submonolayer deposition of a second element on the Pt nanoparticle surface [23–32]. It has been demonstrated that Pt activity for CO electrooxidation depends on the Pt nanoparticle structure [33], the catalyst dispersion and the nature of its support [34]. It has also been shown that CO adsorption and oxidation are site-specific and depend strongly on the surface crystallography [35–48].

The mechanism of the CO oxidation reaction is currently a subject of debate. It is now well established that CO oxidation involves a surface reaction between adsorbed CO and oxidized Pt species at an adjacent site on the surface, the so-called reactant pair as originally proposed by Gilman [49]. However, two different models are invoked to describe the kinetics of this reaction. The first assumes that the reaction proceeds at the perimeter of a water island containing adsorbed OH species in the monolayer of CO and is controlled by the nucleation and growth of these islands [19, 20, 22, 35, 50–54]. The second is the so-called mean-field approximation or Langmuir–Hinshelwood mechanism [36, 42, 55–57], that assumes a

fast surface diffusion of CO_{ads} and OH_{ads} and their mixing at the electrode surface. A more recent version of this mechanism proposes that the oxidation reaction proceeds at specific surface sites (surface defects, kinks, edges, etc.) and both CO_{ads} and OH_{ads} diffuse on the surface to the reaction zone created by these sites [57]. It should be mentioned that spectroscopic data support the nucleation and growth mechanism [53, 54, 58]. Specifically, in situ IR reflectance absorption spectroscopy (IRRAS) played a particularly important role in the studies of CO adsorption and oxidation at Pt surfaces. These efforts are described in a number of recent reviews [59–63]. The literature concerning CO adsorption is vast and this short review quotes only representative references. For an overview see Refs. [64–66].

The adsorption and oxidation of CO at the Pt-solution interface has been investigated exhaustively. In contrast, much less is known about the properties of CO adsorbed at the surface of a Pt catalyst covered by a polymer electrolyte membrane. Osawa et al. [67] provided the first IR-based evidence that CO adsorption at a Pt electrode covered by Nafion film may be different from that at the Pt-solution interface. This work was recently supplemented with new data on CO adsorption at Pt nanoparticles deposited on glassy [68] and dispersed [17] carbon supports covered by Nafion.

The objective of this work is to compare adsorption and oxidation of CO at Pt nanoparticles that are covered by Nafion and that are Nafion-free. With the help of the IRRAS we were able to demonstrate that there are notable differences between the character of CO adsorption and oxidation at Pt nanoparticles covered with and free of the polymer electrolyte membrane. We were able to show that CO oxidation proceeds at higher potentials at Pt nanoparticles covered by the polymer electrolyte membrane. This work complements our earlier IRRAS studies of the interaction of Nafion with a Pt electrode surface [69].

Experimental

The working electrode consisted of Pt nanoparticles deposited onto a polycrystalline Au disk. A modified procedure by Friedrich et al. [18, 33, 34, 70] was used to prepare the electrode. The gold disk was mechanically polished using first 600-, 800- and 1,200-grade sandpaper (Buehler) and next with 1 and 0.3 μm Al_2O_3 powder (Leco). After each polishing stage, the electrode was sonicated in a water–soap mixture for around 0.5 h in an ultrasonic cleaner, and carefully washed with water. Prior to nanoparticle deposition, the electrode was copiously rinsed with ultrapure water and placed in an ozone cleaner (Jelight Co.) for 20 min.

The ozone-cleaned electrode was quickly transferred to a glove box purged with pure argon (BOC Gases), where the Pt nanoparticle deposition was carried out in a water-vapor-free atmosphere. Approximately 10 μl of a colloidal suspension of Pt particles was injected onto the surface of the gold electrode and dried at room temperature for several hours. The electrode was then immersed into pure 2-propanol (Fisher) for about 1 min to remove the nanoparticle stabilizer. The 5% (w/w) solution of Nafion (Aldrich) was diluted with pure 2-propanol (Fisher) to a concentration of 1% (w/w). Ten microliters of this solution was deposited onto the Au surface covered with Pt nanoparticles. The Nafion-coated electrode was then cured at 170 ± 5 °C for 1 h in order to evaporate the solvent and to improve the adhesion between the polymer film and the electrode, as recommended by Ye and Fedkiw [71]. Finally, the electrode was removed from the glove box and immersed into Millipore water for around 24 h prior to electrochemical experiments.

Cyclic voltammograms (CVs) were recorded using a model PG 590 computer-controlled potentiostat (HEKA). A three-electrode Pyrex-glass cell was used for electrochemical experiments. Platinum wire and a saturated calomel electrode (SCE), separated from the cell by a salt bridge, were used as a counter electrode and a reference electrode, respectively. Water purified in a tandem of Milli-Q and Milli-Q plus UV systems (resistivity 18 MΩ) was used to clean the electrodes and glassware and to prepare the supporting electrolyte solutions. The 0.1 M $HClO_4$ supporting electrolyte solution was prepared from ultrapure perchloric acid (Seastar Chemicals). The electrolyte was purged with argon for around 30 min in order to remove oxygen and a blanket of argon was kept over the solution for the duration of the experiment.

The IRRAS spectra were measured using a Nicolet 20SX/C Fourier transform IR apparatus equipped with an MCT-B detector cooled by liquid nitrogen. The sample compartment was purged using CO_2 and H_2O free air from a Puregas Heatless Dryer. The electrode potential was controlled by a PAR 173 potentiostat. The in situ IRRAS experiments were conducted in a syringe-type IR cell with a hemispherical ZnSe window as described in Ref. [72]. *p*-polarized light was used in these experiments. A silver–silver chloride electrode with saturated KCl (SSCE) was the reference electrode (−40 mV versus the SCE). All potentials reported in this work were measured versus the SSCE. The IRRAS spectra were calculated from the ratio of two R_s and R_r taken at sample and reference potentials using the formula:

$$A = \frac{-\log(R_s/R_r) \times 100\%}{S_r},$$

where S_r is the real (electrochemically active) area calculated by integration of the hydrogen desorption peak on the CV.

The reference potentials were chosen as +800 mV for CO (CO was completely oxidized at this potential) and −200 mV for CO_2 (this potential is more negative than the onset potential of the oxidation of CO to CO_2).

CO coverage was calculated as the ratio of the integrated intensity of the CO band in the IRRAS spectrum

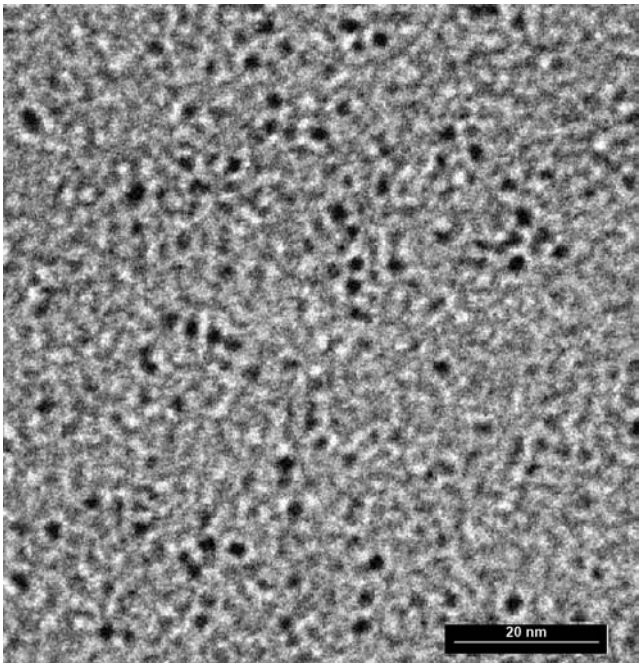

Fig. 1 Transmission electron microscopy (*TEM*) image of Pt nanoparticles reduced using *t*-Bu(Me)$_2$SiH in *N,N*-dimethylacetamide solvent and diluted tenfold for imaging. *Dark spherical shapes* represent nanoparticles calculated to have a mean size of 2.6 ± 0.4 nm

to the maximum value of the integrated band intensity. The maximum intensity of the CO band in the IRRAS spectrum was observed at potentials of 0 and 100 mV for the Nafion-covered and the Nafion-free Pt nanoparticles, respectively. CO was adsorbed on the electrode at $E = -200$ mV by bubbling pure CO (BOC Gases) through the electrolyte for 15 min, followed by purging the electrolyte with argon for 3 h.

Samples for transmission electron microscopy (TEM) imaging of the nanoparticles were prepared inside an inert-gas dry box under an argon atmosphere. Electron microscopy was carried out using a LEO 912AB operating at 100 kV with a liquid nitrogen anticontaminator in place. Digital images were collected using a 1×1 K PROSCAN CCD camera and were processed using the measurement software in the SIS ESIVision program. Both negatively stained (using 2% w/v uranyl acetate) and unstained samples were imaged for measurement comparison. Figure 1 shows an unstained sample where the region of high electron density in each particle is attributed to the platinum.

Results and discussion

Colloid formation and stabilization

Several methods have been used to precipitate colloidal Pt nanoparticles. A citrate-based method was applied by Friedrich and coworkers [18, 33, 34, 70]. Precipitation from a water-in-oil microemulsion was employed by Solla-Gullon and coworkers [72–75], and Gomez et al. [76]. In this work we used a silane-based method that is a modified version of the procedure described by Chung et al. [77]. The Pt nanoparticles were prepared from platinum chloride according to the following reactions: Schemes 1 and 2.

The entire preparation process was carried out in an argon-filled glove box (Mbraun Unilab). First, 8.0 mg (0.03 mmol) platinum chloride (Fisher Scientific Co.) was dissolved in 60 ml *N,N*-dimethylacetamide (DMA, 99 + % from Aldrich, dried and purified by distillation from BaO under reduced pressure), and stirred for 15 min until the platinum chloride dissolved. Then 0.20 ml (140 mg, 1.20 mmol) *t*-BuMe$_2$SiH was added to the mixture and stirring was continued for 24 h. The $PtCl_2$ dissolved in DMA solvent reacted with *t*-BuMe$_2$SiH to form Pt nanoparticles coated with silane and concomitant formation of stoichiometric amounts of hydrogen chloride. This reaction can be considered as autocatalytic, running iteratively until all Pt is in the zero oxidation state and a stable particle size has been reached. It is postulated that the silane coated on the Pt nanoparticles acts as a stabilizer that prevents agglomeration of the nanoparticles [78].

The nature of the stabilization that deters cluster agglomeration of the colloid and prevents precipitation of bulk metal in the DMA/*t*-BuMe$_2$SiH system deserves comment. Previously it has been suggested that this stabilization, which partly manifests itself in particle size, is effected by controlling two processes: nucleation and cluster growth [79, 80]. However, an exact descrip-

Scheme 1

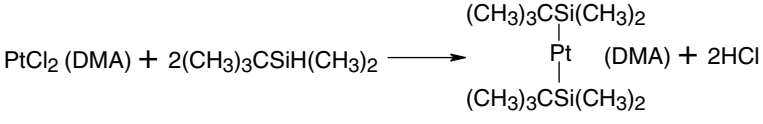

Scheme 2

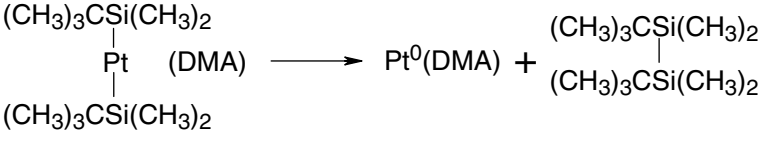

tion of these processes for the colloid used in the electrochemical measurements remains elusive, as an accurate in situ characterization is difficult to achieve. In a $Pd(OAc)_2$/NaOAc derived colloid also formed in DMA and of similar particle size described by Reetz and Westermann [81], an equimolar amount of n-$Bu_4N^+Br^-$ was employed as the stabilizer. Furthermore, a previous study of an electrochemically generated palladium colloid by Reetz et al. [82] that combined high-resolution TEM with scanning tunneling microscopy [82] demonstrated the crucial role of tetraalkyl ammonium salts in stabilizing the nanostructured palladium clusters. The present system however has no added ionic stabilizer, which leads us to conclude that the silane itself is responsible for the apparent stability of the colloid. Our observation that the colloid is only stable against precipitation as bulk metal as long as an excess of silane is present in solution strongly suggests that it plays a critical role beyond its function as the reducing agent in the initial reduction of the platinum salts to Pt(0).

The TEM image in Fig. 1 reveals that the Pt nanoparticles obtained by this method are quasispherical and essentially monodispersed. Figure 2 shows that the Pt nanoparticles are characterized by a narrow size distribution and a mean diameter of 2.6 ± 0.4 nm (0.4 nm is the standard deviation for the distribution of particle sizes over an ensemble of 115 particles). In fact the average size and the size distribution produced by the silane method are similar to the size and distribution of nanoparticles produced by the citrate method [18, 33, 34].

Cyclic voltammetry

The properties of Pt nanoparticles supported at an Au electrode were initially characterized by recording CVs. Curve 1 in Fig. 3 plots a CV for the electrode with freshly deposited Pt nanoparticles without Nafion coating and without cleaning. The curve is featureless, indicating that the Pt surface is blocked by DMA and/or silanes. The Pt_{nano}/Au electrode was then immersed into 2-propanol and then carefully washed with water. The CV was recorded again and the first scan of the CV is shown as curve 2 in Fig. 3. A significant increase of the current was observed. After this treatment, the CV displayed the characteristic hydrogen adsorption/desorption and Pt oxide formation/reduction peaks. Clearly, cleaning in 2-propanol significantly improves the electrochemical activity of Pt nanoparticles. However, a large positive current in the potential region 350–1,280 mV indicates that a residual amount of impurities or adsorbed 2-propanol remained on the surface.

In order to remove these impurities, the electrode potential was continuously cycled between −150 and 1,280 mV. Curve 3 in Fig. 3 plots the CV recorded after 50 oxidation–reduction cycles. This curve has all the features characteristic of a Pt electrode surface; however, the current in the hydrogen adsorption–desorption region significantly decreased, indicating that some of the nanoparticles were detached from the gold support, resulting in a loss of electrochemically active surface area. After repetitive cycling, the Pt oxide reduction peak shifted from around 300 mV (curve 2) to around 450 mV (curve 3). Takasu et al. [83] observed that the position of the Pt oxide reduction peak depends on the size of the Pt nanoparticles and shifts in a positive direction with increasing particle dimension. Therefore, the changes in the CV indicate that cleaning of the catalyst surface by applying repetitive oxidation–reduction cycles leads to aggregation of nanoparticles.

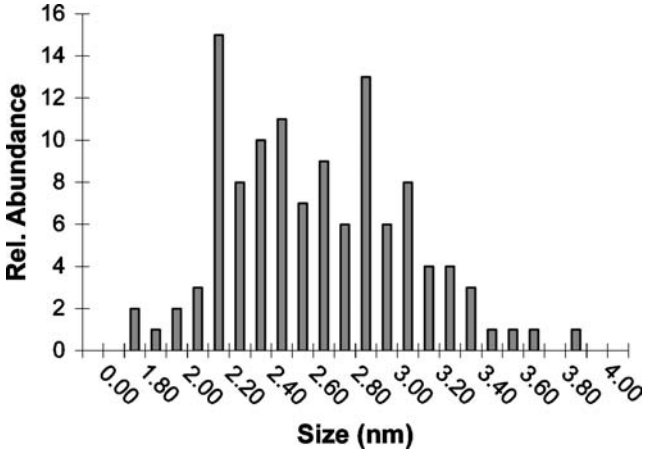

Fig. 2 Histogram of the size distribution of the Pt nanoparticles. In total 115 measurements were obtained from five different TEM images. The majority of the sampled particles fall in the range between 2.0 and 3.2 nm

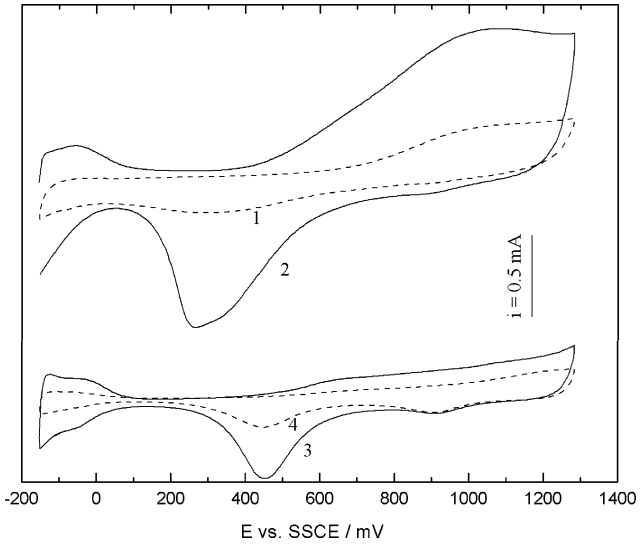

Fig. 3 Cyclic voltammograms in 0.1 M $HClO_4$ recorded at a scan rate 50 mV s^{-1} for freshly deposited Pt nanoparticles onto an Au substrate (*1*), first cycle after immersion into 2-propanol and washing with water (*2*), after potential cycling between −150 and 1,280 mV (50 cycles) (*3*) and after deposition of a Nafion film on the electrode (*4*)

Next, the Nafion film was deposited onto the electrochemically cleaned electrode and the electrode was annealed at 160 °C to improve film adhesion to the gold surface. Curve 4 in Fig. 3 shows the CV recorded for the Nafion-covered electrode after the thermal treatment. Clearly, the voltammetric currents in both the hydrogen adsorption–desorption and the oxide formation–reduction regions decreased significantly, indicating a significant loss of the catalyst reactivity. The Pt electrode area is not significantly reduced by a film of Nafion [67, 69, 84]. Therefore, the significant loss of activity indicates that the thermal treatment resulted in a detachment of nanoparticles from the Au support with a loss of electrical contact. Although the thermal treatment has an adverse effect on the catalyst activity it is necessary. The Nafion films that were not thermally treated were unstable and peeled off of the gold support easily.

In situ IRRAS

In situ IRRAS has been employed to investigate CO adsorption and oxidation at Nafion-coated Pt nanoparticles. For the most negative potential ($E = -200$ mV versus SSCE), Fig. 4 shows IRRAS spectra of CO at Pt-free Au, nanoparticle-covered Au without and with a Nafion film and a polycrystalline Pt disk electrode. In the absence of a Pt catalyst, the IRRAS signal for CO at an Au electrode is very weak and hence IRRAS can be conveniently employed to study adsorption of CO at Pt nanoparticles, using the Au surface as a mirror [33, 67]. The CO spectra show bands of linearly bonded CO. For the Pt nanoparticle electrodes no bands of bridge-bonded CO at around 1,800 cm^{-1} were observed. We note differences between the band shape, position and width. These differences reflect varying electrocatalytic properties of a massive Pt electrode and Pt nanoparticles with and without a film of Nafion. For CO at polycrystalline Pt, the IR band is more symmetric than that for CO adsorbed at Pt nanoparticles. The presence of Nafion causes a broadening and splitting of the band.

The CO band shape, position and width also depend on the electrode potential. Therefore, we examined the evolution of the IR spectra with varying potential before attempting a more thorough band analysis. Figure 5, right, shows IRRAS bands for CO adsorbed at Pt nanoparticles covered by Nafion for electrode potentials ranging from −200 to 750 mV versus the SSCE. In addition, Fig. 5, left, shows the IRRAS bands for CO_2 formed by oxidation of adsorbed CO. The bands change significantly with the applied potential and it is convenient to discuss these changes by analyzing band shape, band position, band width and the integrated band intensity separately.

Starting with the evolution of the band shape with electrode potential, Fig. 6 shows the normalized band intensity (A/A_{max}) versus $\nu_{CO} - \nu_{CO}^{max}$, where A_{max} and ν_{CO}^{max} are the intensity and the frequency at the band maximum, respectively. After such normalization, all bands have the same position and amplitude and one can easily analyze changes in the band shape by superimposing the bands. The bands in panels 1 and 2 correspond to the −200 to +200 mV (SSCE) region, where CO coverage is higher than 0.9. Panels 1 and 2 show bands for Nafion-free and Nafion-covered nanoparticles, respectively. In the absence of Nafion the spectrum consists of one band with a low-frequency shoulder. For all potentials the spectra are fully superimposable.

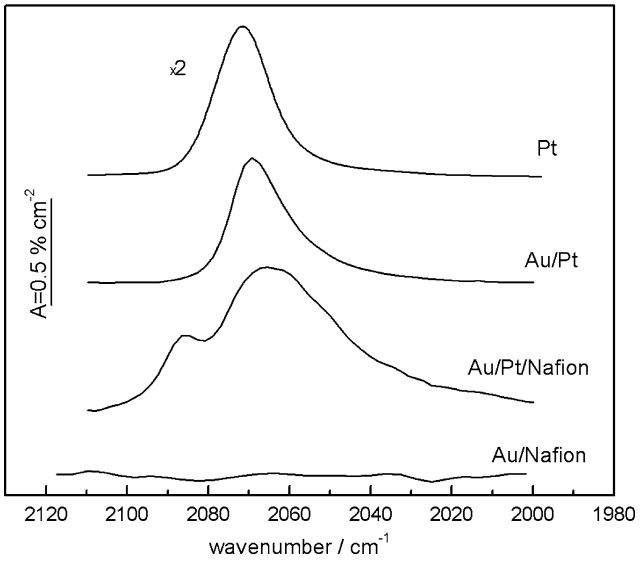

Fig. 4 IR reflectance absorption spectroscopy (*IRRAS*) spectra of CO adsorbed at $E = -200$ V (versus the silver–silver chloride electrode with saturated KCl, *SSCE*) for an Au electrode covered by a film of Nafion, polycrystalline Pt, Pt nanoparticles deposited on Au without Nafion, and Pt nanoparticles deposited on Au with Nafion

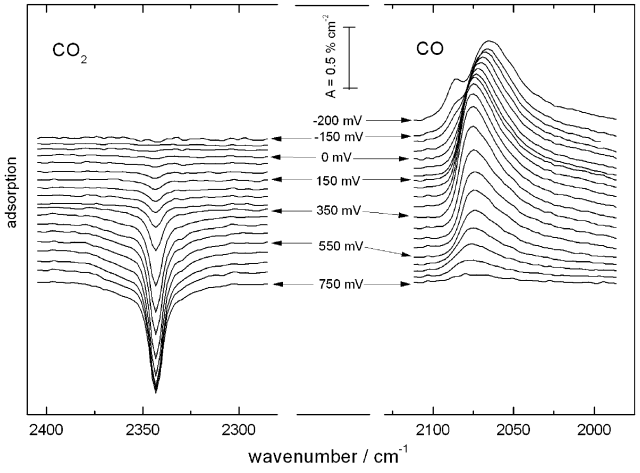

Fig. 5 Background-corrected IRRAS spectra in CO_2 and CO regions for an Au/Pt_{nano}/Nafion electrode. The sample potential changes (from the *top* to the *bottom*) with a step of 50 mV from −200 to 750 mV (for the CO region) and from −150 to 800 mV (for the CO_2 region). The direction of the CO_2 bands is inverted for the benefit of data presentation

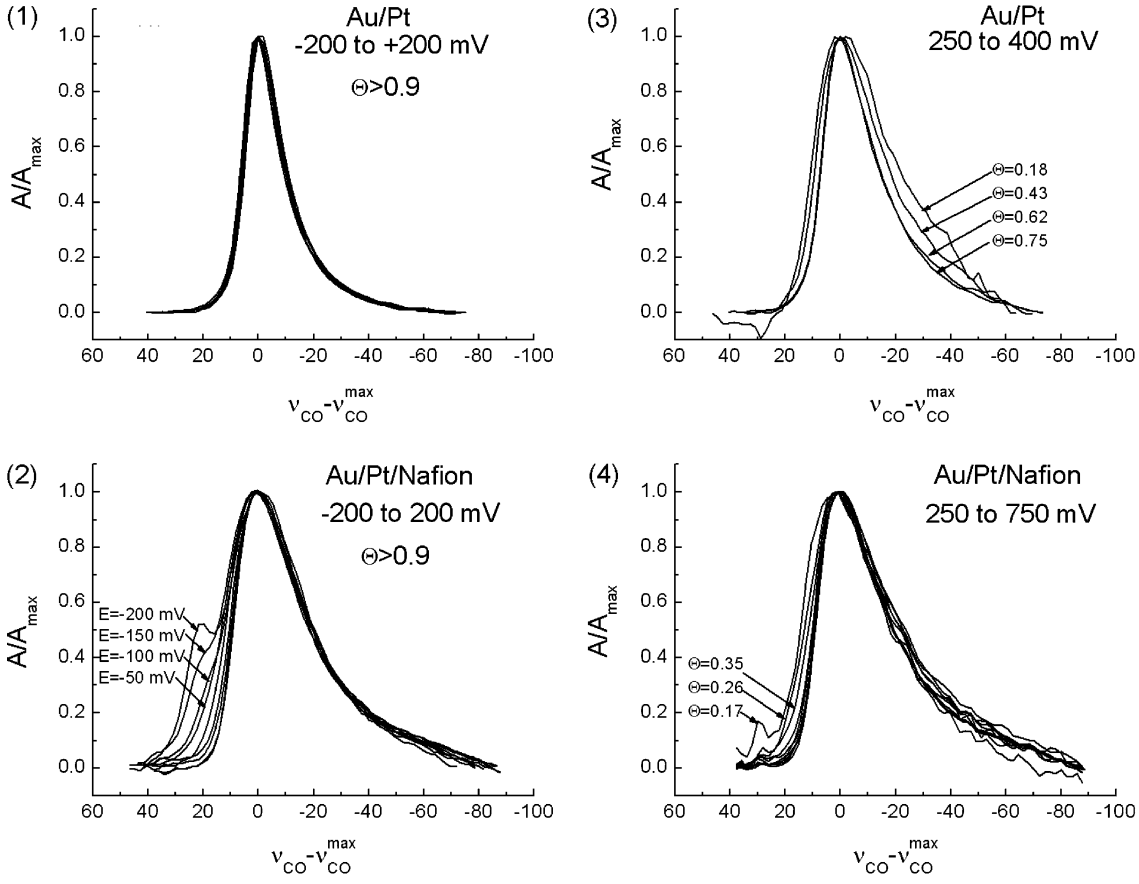

Fig. 6 Normalized background-corrected IRRAS spectra for CO at Au/Pt_{nano} (*1*, *3*) and for CO at Au/Pt_{nano}/Nafion (*2*, *4*) for potentials from −200 to 200 mV (*1*, *2*), from 250 to 400 mV (*2*) and from 250 to 700 mV (*4*)

In contrast, the spectrum of CO at the Nafion-covered electrode displays two overlapping peaks and a very broad shoulder at lower wavenumbers. Similar splitting of the CO band was observed by Osawa et al. [67] for Pt nanoparticles deposited at a Nafion coated Au electrode. Osawa et al. [67] explained such splitting by the presence of regions with a higher and a lower hydronium ion concentration in the Nafion membrane. The higher-frequency band was assigned to Pt nanoparticles in the ion cluster region of the membrane with higher local proton concentration; the lower-frequency band was assigned to nanoparticles in the interfacial region with lower proton concentration. Figure 5, right, shows that the high-frequency peak decreases with increasing potential and merges with the lower-frequency peak at $E \approx 50$ mV (SSCE). This behavior suggests that the nanoparticles experience a more uniform distribution of protons when the potential becomes more positive. Different behavior was observed for nanoparticles produced by electrodeposition at the Nafion-coated Au electrode by Osawa et al. [67]. The CO bands corresponding to high and low proton concentrations were observed at all potentials in that work. However, when nanoparticles are produced by electrodeposition at the Nafion film some of them were formed at the Nafion–solution interface [67]. Consequently, two types of nanoparticles are always present at such an electrode surface. In contrast, all nanoparticles were covered by Nafion in our experiment and only the interaction between Nafion and the Pt surface was affected by the electrode potential.

Panels 3 and 4 of Fig. 6 show normalized bands for $E > 200$ mV (SSCE) where CO coverage was less than 0.9 (panel 3 without Nafion and panel 4 with Nafion). A progressive band broadening is observed when CO coverage decreases at these two electrodes. However, all bands are asymmetric and all have the characteristic broad shoulder at lower frequencies, even the band corresponding to the lowest CO coverage. CO bands of a similar shape were observed by Friedrich et al. [70] for aged electrodes with a broad particle size distribution. The higher-frequency component of such bands was assigned to CO adsorption at aggregated nanoparticles and the lower-frequency component was assigned to CO adsorption at small nanoparticles [33, 71]. Since the oxidation of CO at aggregated nanoparticles proceeds at lower potentials than at smaller particles, a significant change in the band shape with potential was observed in Ref. [70]. In contrast, in our experiments the band shape changes little with CO coverage, suggesting that CO is oxidized at the same rate at all nanoparticles or that we have a relatively narrow particle size distribution.

It is well known that IR bands of CO adsorbed at a Pt catalyst surface arise from collective motions of adsorbed molecules that are ‘‘vibrationally coupled’’ [33,

58, 61, 63]. The strength of the transition dipole moment in the direction normal to the surface (and hence the band intensity) depends on whether these vibrations are in or out of phase [61]. The most intense vibrations are observed when all CO molecules are vibrating in phase. These in-phase modes shift to higher energy when the number of vibrating molecules and their coupling strength increase. The asymmetry of the CO band may therefore be explained by the presence of a distribution of domains of different coupling strength in which the adsorbed CO molecules are present in a similar coordination environment, such as the presence of different facets at the nanoparticle surfaces or domains of different packing density. However, for CO adsorbed at nanoparticles a distortion of a CO band may also be a result of the optical properties of the film of nanoparticles [85–87]. For nanoparticles covered by Nafion an additional distortion may be caused by the optical properties of the polyelectrolyte film [88]. However, Nafion does not absorb IR photons at the frequencies of CO bands [67, 69] and hence the latter effect is most likely negligible.

Figure 7 shows the frequency of the CO band maximum as a function of the electrode potential for the massive polycrystalline Pt, Au covered by Pt nanoparticles and an Au/Pt nanoparticle electrode covered by Nafion. Within the range of potentials corresponding to full coverage of the catalyst surface by CO, the band maximum displays a linear dependence on E with a Stark tuning rate of around 30 cm^{-1} V^{-1}, consistent with the literature [25, 58, 89, 90]. At potentials where CO coverage drops below unity, the frequency becomes either independent of or decreases with the potential (or with decreasing coverage). This behavior was frequently reported in the literature [25, 33, 58]. With decreasing coverage, the dipole coupling strength decreases and the band shifts to lower frequencies [58].

The frequency of the band for CO adsorbed at the Au electrode with nanoparticles without Nafion displays a particularly strong redshift with decreasing coverage. This behavior may be understood by looking at the plot of the full width at half maximum (FWHM) of the CO band for the three electrodes, shown in Fig. 8. For the polycrystalline Pt electrode, the FWHM is around 14–15 cm^{-1} and is almost independent of the electrode potential and CO coverage. Similar behavior was observed for CO-stripping from a Pt(111) electrode by Chang and Weaver [58]. This indicates that CO oxidation at polycrystalline Pt involves the island formation and growth mechanism such that the coordination environment of CO molecules within islands remains essentially unchanged with coverage.

In contrast, the oxidation of CO at the Au/Pt nanoparticles electrode without Nafion displays a dramatic increase of the band width from around 16 cm^{-1} at Θ = 1 to around 32 cm^{-1} at Θ = 0.18. A similar change of the band width was observed in Ref. [58] for a CO monolayer formed by dosing CO to an initially CO-free Pt(111) surface. Such significant band broadening is indicative of the formation of highly dispersed small islands of CO. This behavior correlates very well with the downshift of the band position observed in Fig. 7. The strength of the vibrational dipole coupling is expected to decrease significantly if adsorbed CO is dispersed into small domains. Consequently, the band broadening is expected to be accompanied by a parallel downshift of the band position.

The FWHM for CO adsorbed at Pt nanoparticles covered by Nafion is much larger and changes only from around 30 to 35 cm^{-1} . At full coverage the width of the band is increased owing to the presence of an additional high-frequency band, tentatively assigned to the regions of the Nafion film with a higher proton concentration. Since this additional peak disappears at more positive

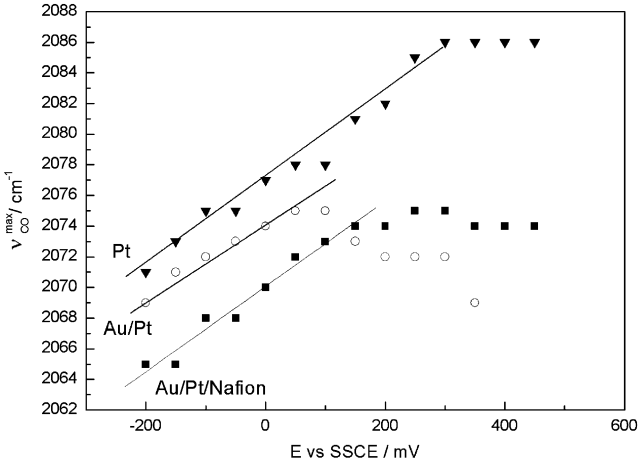

Fig. 7 Frequency at the CO band maximum versus the electrode potential for Au/Pt_{nano}/Nafion (*squares*), Au/Pt_{nano} (*circles*) and polycrystalline Pt (*triangles*)

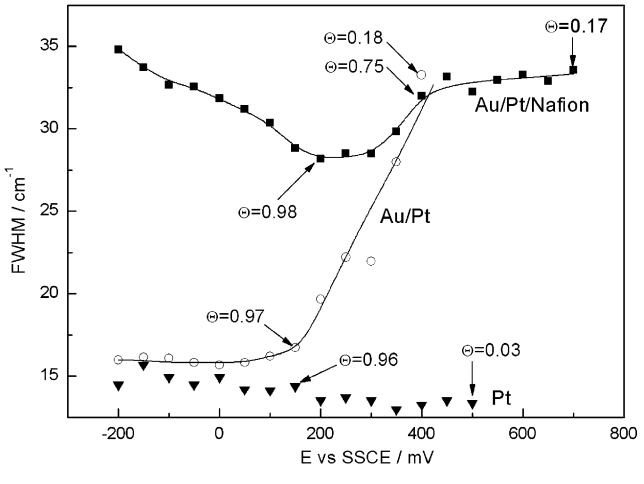

Fig. 8 Full width at half maximum of the CO band against the electrode potential for Au/Pt_{nano}/Nafion (*squares*), Au/Pt_{nano} (*circles*) and polycrystalline Pt (*triangles*)

potentials, the band becomes narrower. The band becomes broader again with the onset of the oxidative stripping of CO. In this range of potentials the band width for CO adsorbed at nanoparticles covered by Nafion becomes equal to the band width for CO adsorbed at nanoparticles without Nafion.

The significant differences between the changes of the CO band width during the oxidative stripping suggest that the mechanisms of the oxidation reaction at the bulk polycrystalline Pt and the Pt nanoparticles electrodes are different. We have already mentioned that the behavior of the CO band at polycrystalline Pt is consistent with the island formation and growth mechanism [35, 62]. In contrast, significant dispersion of adsorbed CO during the oxidative stripping is more consistent with the Langmuir–Hinshelwood mechanism [36, 55–57].

The oxidation of adsorbed CO requires that water molecules penetrate the dense CO adlayer, providing oxygen needed for the conversion of CO to CO_2. This reaction is slower for adlayers that display stronger dipolar coupling [58, 61]. For the three Pt electrodes, Fig. 9 shows the change of normalized integrated intensities of CO and CO_2 bands as a function of the electrode potential. The dipolar coupling is stronger at polycrystalline CO than at Au/Pt nanoparticles without Nafion and indeed the oxidation of CO starts at more positive potentials at the massive Pt electrode. The situation is more complex for the Au/Pt nanoparticles covered by Nafion. The oxidation starts at more negative potentials than at the polycrystalline Pt but the changes of the CO band intensity with potential are more gradual; however, this more gradual change may be due to the presence of residual CO in the bulk of the Nafion membrane. Indeed, the integrated CO_2 band intensity (not normalized) was much higher for the Au/Pt/Nafion electrode than for the Au/Pt electrode, which confirms that a residual CO molecule was trapped in the Nafion membrane and is it much more difficult to remove CO from the membrane by purging with Ar than to remove CO from the electrolyte solution. Significantly, the oxidation of CO is observed at more positive potentials than at the Nafion-free nanoparticles. This behavior suggests that Nafion slows down oxidation of CO. This result is consistent with the recent studies of HCOOH oxidation at the Nafion-covered Pt electrode by McGovern et al. [84], who demonstrated that a film of Nafion slows down the HCOOH oxidation reaction as well.

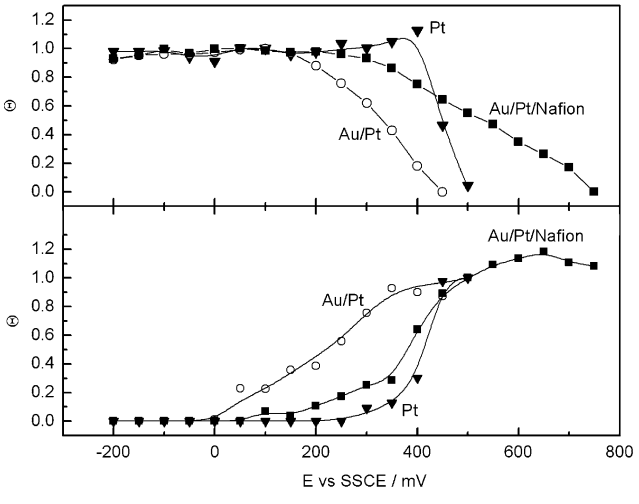

Fig. 9 Normalized integrated band intensity Θ versus the electrode potential for Au/Pt_{nano}/Nafion (*squares*), Au/Pt_{nano} (*circles*) and polycrystalline Pt (*triangles*). *Top*: Θ for CO calculated by dividing the integrated band intensity at a given E by the integrated intensity of the band at $E = 0.1$ V (SSCE). *Bottom*: Θ for CO_2 calculated by dividing the integrated band intensity at a given E by the integrated intensity of the band at $E = 0.5$ V (SSCE)

Summary and conclusions

We have synthesized colloidal Pt nanoparticles with a mean particle size of 2.6 ± 0.4 nm by reducing $PtCl_2$ dissolved in DMA with t-$BuMe_2SiH$. The latter compound acted both as a reducing agent and a stabilizer of Pt nanoparticles. Pt nanoparticles were deposited onto the Au substrate and in situ IRRAS was applied to investigate CO adsorption and oxidation at the surface of the catalyst. The reactivity of nanoparticles covered by Nafion was compared with the reactivity of nanoparticles without a film of Nafion. We found that CO oxidation proceeds at lower overpotentials at nanoparticles than at polycrystalline Pt. The IRRAS data indicate that the difference in the reactivity may be explained by a different mechanism of the oxidation reaction: Langmuir–Hinshelwood at Pt nanoparticles and island formation and growth at polycrystalline Pt. We have also observed that a film of Nafion slows down the CO oxidation reaction. Finally, Pt nanoparticles produced by reduction with silane display better catalytic properties than nanoparticles produced by reduction with citrate [18]. Our results are preliminary in nature. Further studies of the effect of particle size and a comparison with nanoparticles produced by the citrate method are currently under way.

Acknowledgements We acknowledge financial support by the Natural Sciences and Engineering Council of Canada (NSERC). J.L. acknowledges the Canada Foundation for Innovation for the Canada Research Chair Award. Electron Microscopy was performed by Robert Harris in the NSERC Guelph Regional STRM Facility, which is partially funded by an NSERC Major Facility Access Grant.

References

1. Ralph TR, Hogarth MP (2002) Platinum Metals Rev 46:117
2. Hogarth MP, Ralph TR (2002) Platinum Metals Rev 46:146
3. Larminie J, Dicks A (2000) Fuel cell systems explained. Wiley, New York
4. Gasteiger HA, Markovic N, Ross PN Jr, Cairns EJ (1994) J Phys Chem 98:617

5. Wang K, Gasteiger HA, Markovic NM, Ross PN Jr (1996) Electrochim Acta 41:2587
6. Hayden BE (1997) Catal Today 38:473
7. Lin WF, Iwasita T, Vielstich W (1999) J Phys Chem 103:3250
8. Watanabe M, Motoo S (1975) J Electroanal Chem 60:275
9. Schmidt TJ, Stamencovic V, Markovic N, Ross PN (2003) Electrochim Acta 48:3823
10. Diemant T, Hager T, Hoster HE, Rauscher H, Behm RJ (2003) Surf Sci 541:137
11. Lucas CA, Markovic NM, Grgur BN, Ross PN (2000) Surf Sci 448:65
12. Igarashi H, Takeshi F, Zhu Y, Uchida H, Watanabe M (2001) Phys Chem Chem Phys 3:306
13. Jusys Z, Schmidt TJ, Dubau L, Lasch K, Jorissen L, Garche J, Behm RJ (2002) J Pow Sour 105:297
14. Lima A, Coutanceau C, Leger J-M, Lamy C (2001) J Appl Electrochem 31:379
15. Takasu Y, Iwasaki T, Sugimoto W, Murakami Y (2000) Electrochem Comm 2:671
16. Frelink T, Visscher W, van Veen JAR (1995) J Electroanal Chem 382:65
17. Rice C, Tong YY, Oldfield E, Wieckowski A, Hahn F, Gloaguen F, Leger JM, Lamy C (2000) J Phys Chem 104:5803
18. Friedrich KA, Henglein F, Stimming U, Unkauf W (2000) Electrochim Acta 45:3283
19. Maillard F, Eikerling M, Cherstiouk OV, Schreier S, Savinova E, Stimming U (2004) Faraday Discussions 125:357
20. Maillard F, Savinova ER, Simonov PA, Zaikovskii VI, Stimming U (2004) J Phys Chem B (submitted)
21. Cherstiouk OV, Simonov PA, Savinova ER (2003) Electrochim Acta 48:3851
22. Cherstiouk OV, Simonov PA, Zaikovskii VI, Savinova ER (2003) J Electroanal Chem 554–555:241
23. Brankovic SR, Wang JX, Adzic RR (2001) Elctrochem Solid State Lett 4:A217
24. Park S, Wieckowski A, Weaver MJ (2003) J Am Chem Soc 125:2282
25. Lin WF, Zei MS, Eiswirth M, Ertl G, Iwasita T, Vielstich W (1999) J Phys Chem 103:6968
26. Gomez R, Rodes A, Perez JM, Feliu JM, Aldaz A (1995) Surf Sci 344:85
27. Lu GQ, Waszczuk P, Wieckowski A (2002) J Electroanal Chem 532:49
28. Lu GQ, White J, Wieckowski A (2004) Surface Sci 564:131
29. Tong YY, Kim HS, Babu PK, Waszczuk P, Wieckowski A, Oldfield E (2002) J Am Chem Soc 124:468
30. Yee N, Chottiner GS, Scherson D (2004) J Phys Chem B 108:5847
31. Alvarez B, Rodes A, Perez JM, Feliu JM (2003) J Phys Chem 107:2018
32. Schubert MM, Kahlich MJ, Feldmeyer G, Huttner M, Hackenberg S, Gasteiger HA, Behm RJ (2001) Phys Chem Chem Phys 3:1123
33. Friedrich KA, Henglein F, Stimming U, Unkauf W (1998) Coll Surf A 134:193
34. Friedrich KA, Marmann A, Stimming U, Unkauf W, Vogel R (1997) Fresenius J Anal Chem 358:163
35. Love B, Lipkowski J (1988) ACS Symp Ser 378:484
36. Lebedeva NP, Koper MTM, Feliu JM, van Santen RA (2002) J Phys Chem 106:12938
37. Lebedeva NP, Koper MTM, Herrero E, Feliu JM, van Santen RA (2000) J Electroanal Chem 487:37
38. Climent V, Gómez R, Feliu J (1999) Electrochim Acta 45:629
39. Herrero E, Alvarez B, Feliu JM, Blais S, Radovic-Hrapovic Z, Jerkiewicz G (2004) J Electroanal Chem 567:139
40. Lucas CA, Markovic NM, Ross PN (1999) Surf Sci 425:L381
41. Baldelli S, Markovic N, Ross PN, Shen YR, Somorjai G (1999) J Phys Chem B 103:8920
42. Petukhov AV, Akermann W, Friedrich KA, Stimming U (1998) Surf Sci 404:182
43. Akemann W, Friedrich KA, Linke U, Stimming U (1998) Surf Sci 404:571
44. Markovic NM, Grgur BN, Lucas CA, Ross PN (1997) Surf Sci 384:L805
45. Kim CS, Tornquist WJ, Korzeniewski C (1994) J Chem Phys 101:9113
46. Kim CS, Korzeniewski C (1997) Anal Chem 69:2349
47. Palaikis L, Zurawski D, Hourani M, Wieckowski A (1988) Surface Sci 199:183
48. Leung L-WH, Wieckowski A,Weaver MJ (1988) J Phys Chem 92:6985
49. Gilman S (1964) J Phys Chem 68:70
50. Feliu JM, Orts JM, Femandez-Vega A, Aldaz A, Clavilier J (1990) J Electroanal Chem 296:191
51. Orts JM, Louis E, Sander LM, Feliu JM, Aldaz A, Clavilier J (1998) Surf Sci 416:371
52. Orts JM, Louis E, Sander LM, Clavilier J (1998) Electrochim Acta 44:1221
53. Pozniak B, Mo Y, Scherson DA (2002) Faraday Discussions 121:313
54. Pozniak B, Scherson DA (2004) In: Paper presented at the international conference on electrified interfaces, Spa, Belgium, 10–17 July 2004
55. Koper MTM, Jansen APJ, van Santen RA, Lukkien JJ, Hilbers PAJ (1998) J Chem Phys 109:6051
56. Lebedeva NP, Koper MTM, Feliu JM, van Santen RA (2002) J Electroanal Chem 524–525:242
57. Koper MTM, Lebedeva NP, Hermse CGM (2002) Faraday Discussions 121:301
58. Chang SC, Weaver MJ (1990) J Chem Phys 92:4582
59. Korzeniewski C, Severson MW (1995) Spectrochim Acta 51A:499
60. Korzeniewski C (1997) Crit Rev Anal Chem 27:81
61. Korzeniewski C (1999) Vibrational coupling effects on infrared spectra of adsorbates on electrodes. In: Wieckowski A (ed) Interfacial electrochemistry, Chap 20. Dekker, New York, pp 345–352
62. Iwasita T, Nart FC (1997) Prog Surf Sci 55:271
63. Weaver MJ, Zou S (1998) In: Clark RJH, Hester RE (eds) Advances in spectroscopy, vol 26. Wiley, Chichester
64. Markovic NM, Ross PN (2002) Surf Sci Rep 45:121
65. Waszczuk P, Lu G, Wieckowski A, Lu C, Rice C, Masel RI (2002) Electrochim Acta 47:3637
66. Park S, Wasilewski SA, Weaver MJ (2002) Electrochim Acta 47:3611
67. Osawa M, Nakane T, Ito K, Suetaka W (1989) J Electroanal Chem 270:459
68. Chen W, Sun S-G, Zhou Z-Y, Chen S-P (2003) J Phys Chem B 107:9808
69. Malevich D, Zamlynny V, Sun S-G, Lipkowski J (2003) Z Phys Chem 217:513
70. Friedrich KA, Henglein F, Stimming U, Unkauf W (2001) Electrochim Acta 47:689
71. Ye J-H, Fedkiw PS (1995) Electrochim Acta 40:291
72. Solla-Gullon J, Montiel V, Aldaz A, Clavilier J (2000) J Electroanal Chem 491:69
73. Solla-Gullon J, Montiel V, Aldaz A, Clavilier (2002) J Electrochem Comm 4:716
74. Solla-Gullon J, Montiel V, Aldaz A, Clavilier J (2003) J Electrochem Soc 150:E104
75. Solla-Gullón J, Rodes A, Montiel V, Aldaz A Clavilier J (2003) J Electroanal Chem 554–555:273
76. Gomez R, Perez JR, Solla-Gullon J, Montiel V, Aldaz A (2004) J Phys Chem B 108:9943
77. Chung MK, Orlova G, Goddard JD, Schlaf M, Harris R, Beaveridge TJ, White G, Hallet FR (2002) J Am Chem Soc 124:10508
78. Chung MK, Schlaf M (2004) J Am Chem Soc 126:7386
79. Aiken III JD, Finke RG (1999) J Mol Catal A 145:1
80. Bradley JS, Tesche B, Busser W, Maase M, Reetz MT (2000) J Am Chem Soc 122:4631
81. Reetz MT, Westermann E (2000) Angew Chem 39:165
82. Reetz MT, Helbig W, Quaiser SA, Stimming U, Breuer N, Vogel R (1995) Science 267:367

83. Takasu Y, Ohashi N, Zhang X-G, Murakami Y, Minagawa H, Sato S, Yahikozawa K (1996) Electrochim Acta 41:2595
84. McGovern MS, Garnett EC, Rice C, Masel RI, Wieckowski A (2003) J Power Sources 115:35
85. Pecharronan C, Cuesta A, Gutierrez C (2002) J Electroanal Chem 529:145
86. Pecharronan C, Cuesta A, Gutierrez C (2004) J Electroanal Chem 563:91
87. Bjerke AE, Griffith PR, Theiss W (1999) Anal Chem 71:1967
88. Porter MD (1988) Anal Chem 60:1143A
89. Kunimatsu K, Seki H, Golden WG, Gordon JP, Philpott MR (1985) Surf Sci 158:596
90. Park S, Wasilewski SA, Weaver MJ (2001) J Phys Chem 105:9719